Cyclicity in the middle Eocene central Arctic Ocean sediment record: Orbital forcing and environmental response

Francesca Sangiorgi,[1,2] Els E. van Soelen,[1] David J. A. Spofforth,[3] Heiko Pälike,[3] Catherine E. Stickley,[4] Kristen St. John,[5] Nalan Koç,[4,6] Stefan Schouten,[2] Jaap S. Sinninghe Damsté,[2] and Henk Brinkhuis[1]

Received 30 April 2007; revised 19 September 2007; accepted 6 November 2007; published 22 March 2008.

[1] Continuous X-ray fluorescence scanning of middle Eocene (~46 Ma) core M0002A-55X (~236–241 m composite depth), recovered during Integrated Ocean Drilling Program Expedition 302, revealed a strong cyclical signal in some major and trace geochemical elements. We performed a multiproxy study of the same core, which included organic geochemical, sedimentological, and biological parameters, and integrated our results with available geochemical and physical properties data. The target was to look for cyclicity in the several proxies, investigate their frequency, and understand the environmental response to the potential forcing. Results indicate that a higher terrigenous component corresponds to lower organic carbon concentration, smaller contributions by angiosperm pollen and spores, organic-walled dinoflagellate cysts, and chrysophyte cysts (lower productivity, shorter growing season for flowering plants, and lower stratification) but higher contributions by bisaccate pollen and diatoms (drier conditions on land, more marine conditions) and higher terrigenous sand (ice-rafted debris (IRD)). Our investigation shows that physical proxy parameters hold cyclicity with periods of about 50 and 100 cm and that these frequency components are compatible with a Milankovitch-type orbital forcing, representing precession and obliquity, respectively. The longer 100 cm cyclicity is also present in the biological (pollen, dinoflagellate cysts, and siliceous microfossils) and in the sedimentological (IRD) proxies. The environmental signal derived from the integrated multiproxy analysis suggests that in an enclosed Arctic Ocean at time of ice (sea ice and glacial ice) initiation the biological proxies responded more strongly to growing season length/darkness, whereas the terrigenous components, directly driven by sea ice and/or glacial ice formation and extent, responded more directly to seasonal insolation.

Citation: Sangiorgi, F., E. E. van Soelen, D. J. A. Spofforth, H. Pälike, C. E. Stickley, K. St. John, N. Koç, S. Schouten, J. S. Sinninghe Damsté, and H. Brinkhuis (2008), Cyclicity in the middle Eocene central Arctic Ocean sediment record: Orbital forcing and environmental response, *Paleoceanography*, *23*, PA1S08, doi:10.1029/2007PA001487.

1. Introduction

[2] The modern Arctic Ocean is almost entirely surrounded by land, with shallow connections to the Pacific Ocean through the Bering Strait and to the Atlantic Ocean through the Canadian Archipelago and Barents Sea, and a deeper gateway through the Fram Strait. The pan-Arctic drainage basin covers an area of about 1.5 times that of the Arctic Ocean [*Lammers et al.*, 2001] and four of the world's major river systems discharge into the basin [*Aagaard and Carmack*, 1989; *Meincke et al.*, 1997; *Serreze et al.*, 2006]. Precipitation in the area exceeds evapotranspiration, river runoff can be as high as 3200 km^3/a, and the annual freshwater balance in the basin is positive, with the Fram Strait representing one of the major freshwater sinks [*Serreze et al.*, 2006]. Several components of the modern Arctic hydrological cycle show prominent annual cycles. Net precipitation peaks in late summer to early autumn [*Walsh et al.*, 1994], rivers show strong spring maximum [*Lammers et al.*, 2001], and the ice flux through the Fram Strait peaks in winter [*Vinje*, 2001], reflecting seasonality in the atmospheric circulation. Models for time intervals conducive for glaciations show that the atmospheric component of the high-latitude freshwater balance is dominated by the effect of obliquity and is maximized when obliquity is low [*Jackson and Broccoli*, 2003].

[3] During the middle Eocene, the Arctic Ocean was even more enclosed than it is today. The Fram Strait, which represents the unique deep connection to the world oceans, was not fully developed until the early Miocene [*Jakobsson et al.*, 2007]. The middle Eocene temperatures indicate a warm Arctic environment, with Mean Annual Temperature (MAT) between ~8 and 15°C, and winter temperatures around 0°C [*Greenwood and Wing*, 1995; *Jahren and Sternberg*, 2003, and references therein; *Brinkhuis et al.*,

[1]Palaeoecology, Laboratory of Palaeobotany and Palynology, Institute of Environmental Biology, Utrecht University, Utrecht, Netherlands.
[2]Department of Marine Biogeochemistry and Toxicology, Royal Netherlands Institute for Sea Research, Den Burg, Netherlands.
[3]School of Ocean and Earth Science, University of Southampton, Southampton, UK.
[4]Norwegian Polar Institute, Tromsø, Norway.
[5]Department of Geology and Environmental Science, James Madison University, Harrisonburg, Virginia, USA.
[6]Department of Geology, University of Tromsø, Tromsø, Norway.

0883-8305/08/2007PA001487$12.00

2006; *Sangiorgi et al.*, 2008]. The inferred thermal seasonality was thus moderate, the hydrological cycles intensified, and the humidity was approximately double that of today [*Greenwood and Wing*, 1995; *Jahren and Sternberg*, 2003]. Higher humidity and higher precipitation must have heavily affected the land-locked Arctic Ocean and surface waters must have been fresher than today. Indeed, the Palaeogene sedimentary record recovered at the Lomonosov Ridge (central Arctic Ocean) during Integrated Ocean Drilling Program (IODP) Expedition 302 (Arctic Coring Expedition (ACEX)) indicates that the Arctic Ocean was predominantly characterized by surface fresh to brackish waters [*Expedition 302 Scientists*, 2006; *Moran et al.*, 2006; *Sangiorgi et al.*, 2008; *Stickley et al.*, 2008; *Waddell and Moore*, 2008]. Episodes of extreme fresh surface waters in the Arctic Ocean, which allowed blooming of the freshwater fern *Azolla*, have been shown for the middle Eocene, at ~49 Ma [*Brinkhuis et al.*, 2006]. Moreover, cyclic fluctuations in the *Azolla* concentrations in ACEX record seem to be driven by orbital forcing, suggesting that periodical freshening of the Arctic Ocean was astronomically modulated.

[4] Spectral analysis of climate proxy records have provided substantial evidence that a fraction of the climatic variance is driven by insolation changes in the frequency ranges of obliquity and precession [e.g., *Hays et al.*, 1976], and obliquity affects the strength in seasonality. Seasonality was probably weaker than today in the warmer middle Eocene [e.g., *Greenwood and Wing*, 1995]. However, it must have been still important for the Arctic and the high latitudes, which experience long dark winters.

[5] Seasonality (and increase in seasonality) may have also played an important role during the long Eocene cooling trend in determining the timing of the transition from a greenhouse to an icehouse world for higher latitudes. In fact, this long-term cooling trend seems to have involved mainly the poles, as low-latitude climate remained stable and warmer than today until the Oligocene [e.g., *Pearson et al.*, 2007]. Continental glaciers were likely already present in Greenland [*Eldrett et al.*, 2007] by at the latest the late Eocene, and direct evidences for ice presence in the Arctic Ocean point to a middle Eocene age [*Expedition 302 Scientists*, 2006; *Moran et al.*, 2006; *St. John*, 2008].

[6] This study is directed from a strong cyclical signal in some major and trace geochemical elements (e.g., Fe, K, Ti, Al, Si) recorded during continuous X-ray fluorescence (XRF) scanning of middle Eocene ACEX core M0002A-55X (D. J. A. Spofforth et al., Paleogene record of elemental concentrations in sediments from the Arctic Ocean obtained by XRF analysis, submitted to *Paleoceanography*, 2007, hereinafter referred to as Spofforth et al., submitted manuscript, 2007). Besides containing a strong cyclicity signal, this core is also the oldest where high abundance of terrigenous sand (likely related to ice-rafted debris, IRD) has been found [*St. John*, 2008]. We performed a multiproxy palynological (dinoflagellate cysts, pollen and spores), micropaleontological (siliceous microfossils), sedimentological (terrigenous sand abundance) and geochemical study to test whether the cyclicity identified in the XRF scanning also held for other proxies. The aim was to investigate the cycle's frequency and to understand the response of the Arctic environment to the orbital forcing at time of ice initiation in the Arctic Ocean.

2. Material and Methods

[7] Samples analyzed were taken from core M0002A-55X (~236.07–241.38 m composite depth (mcd)), which is part of unit 2 of the ACEX core drilled from the Lomonosov Ridge (Figure 1) [*Expedition 302 Scientists*, 2006]. Lithologic unit 2 (223.56–313.61 mcd) is a mud-bearing biosiliceous ooze, characterized by submillimeter laminations, total organic carbon (TOC) contents of about 2–3% and high values of OC of algal origin [*Expedition 302 Scientists*, 2006; *Stein et al.*, 2006]. Unexpectedly, the upper ~20 m of unit 2 also contain fluctuating abundances of quartz-dominated terrigenous sands [*St. John*, 2008] and granules/pebbles [*Expedition 302 Scientists*, 2006; A. Krylov, personal communication, 2007]. Given their occurrence on a high-latitude isolated bathymetric high (Lomonosov Ridge), these particles are interpreted as ice-rafted debris (IRD). Details on the lithological units are given elsewhere [*Expedition 302 Scientists*, 2006].

[8] According to the available age model [see *Backman et al.*, 2008], core M0002A-55X has a middle Eocene age (~46 Ma) and belongs to a section of the ACEX record where sedimentation rate is 24.3 m/Ma.

2.1. XRF Scanning

[9] The X-ray Fluorescence (XRF) chemical element data were collected using the AVAATECH X-ray core scanner at the Bremen ODP Core Repository (BCR) and calibrated using total sediment digestion of discrete samples. The XRF core scanner is a rapid and nondestructive system for obtaining nearly continuous and high-resolution analyses of a suite of elements at the surface of split cores [*Jansen et al.*, 1998]. We determined elemental counts for Al, Si, P, S, K, Ca, Ti, Mn, Fe using parameters of 280 μA, 10 KV and a 30 s count time. Sampling resolution was based on shipboard MST measurements giving a sample spacing of 3 cm through this core with a scanning surface area of ~1 cm^2 (equivalent to ~0.5 ka). Where necessary the sampling plan was adjusted to avoid core gaps and disturbances. XRF calibration to sediment concentrations were carried out using the $LiBO_2$ alkali fusion method [*Totland et al.*, 1992] and run on an ICP-MS. Further details on the scanning procedure and fusion method is given by Spofforth et al. (submitted manuscript, 2007).

2.2. Palynology

[10] Forty-one samples from unit 2 core M0002A-55X (236.27–241.10 mcd) were selected for palynological analysis, at resolutions of 5–25 cm (~2–10 ka). Samples were processed as outlined by *Wood et al.* [1996] with no oxidation. Assemblages were counted using a light microscope at a magnification of 400. Dinoflagellate cysts (dinocysts) were identified to species level when possible following [*Fensome and Williams*, 2004]. Other palynomorphs (bisaccate pollen, *Taxodium* pollen, angiosperm pollen, spores, acritarchs, freshwater algae/algal remains such as *Pediastrum*, *Tasmanites*, *Cymatiosphaera* spp., *Pterospermella*) were also counted. Percentages and con-

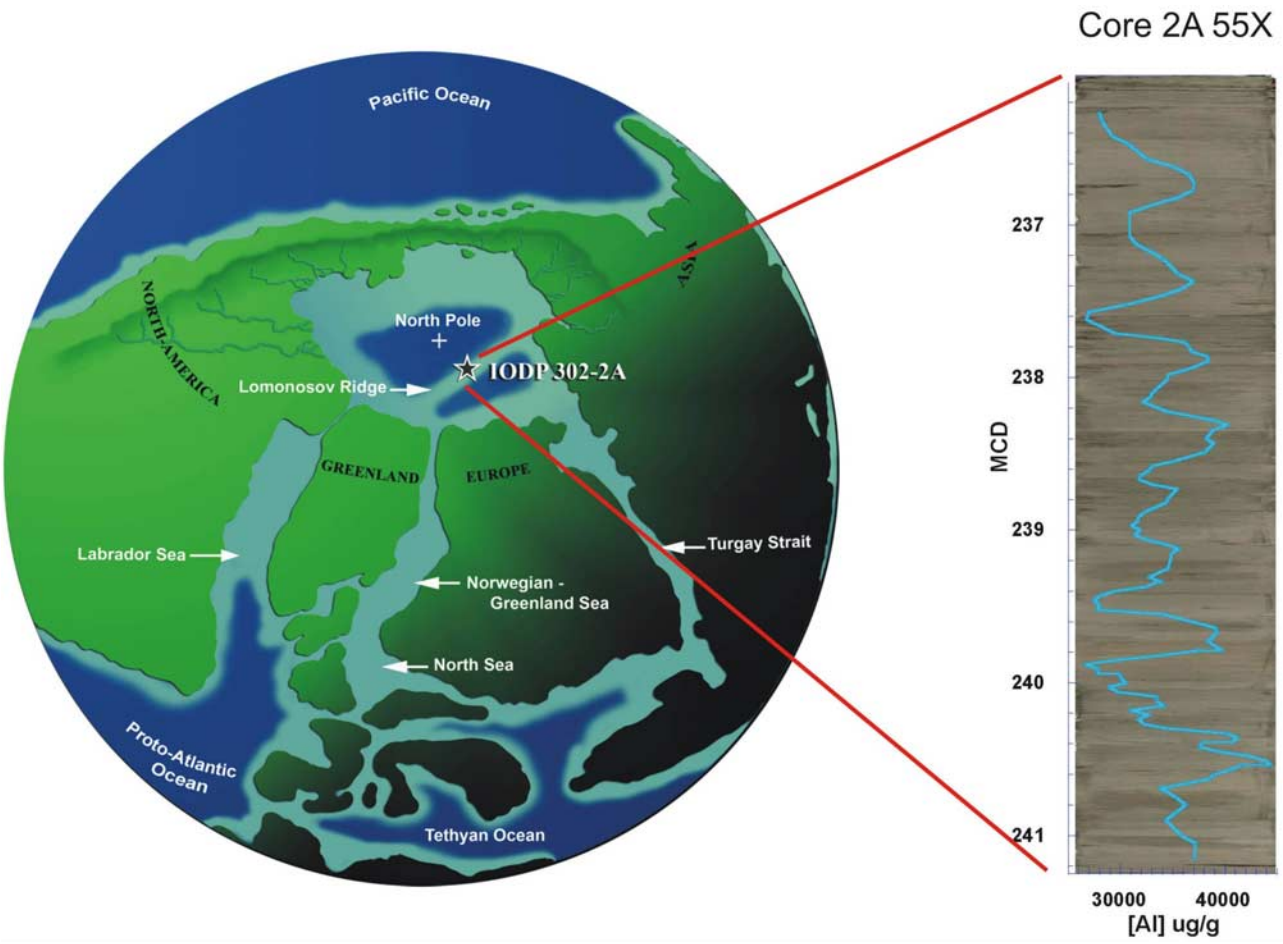

Figure 1. (left) Location of Integrated Ocean Drilling Program (IODP) Hole 302 2A on the paleogeographic reconstruction of the Arctic Ocean at middle Eocene (~50 Ma) (modified from *Brinkhuis et al.* [2006]). (right) Image of core 302-2A-55X, showing overimposed Al (μg/g) concentration profile.

centrations of each group were calculated. Percentages of angiosperm pollen, spores and of bisaccate pollen have been calculated on the total terrestrial palynomorphs (total pollen and spores). Total dinocyst percentages are calculated relative to the total palynomorphs, while individual dinocyst genus percentages are calculated on the total dinocysts counted.

2.3. Siliceous Microfossils

[11] Twenty-seven samples between 236.19 and 241.32 mcd at an average resolution of 20 cm (~10 ka) were analyzed. Silica-selective processing and analyses were carried out at the Norwegian Polar Institute, Tromsø requiring only oxidation of organic matter (hot 30% hydrogen peroxide) and removal of clays (settling and centrifugation). For quantitative analysis, 1 ml of divinylbenzene microspheres (concentration 3.28×10^6 spheres/ml) was added to each of the digested samples prior to slide preparation, following the methods of *Battarbee and Kneen* [1982] and *Battarbee* [2001]. Slides were analyzed for their siliceous microfossil content at a magnification of 1000. Siliceous microfossil groups encountered and tallied are: diatoms, chrysophyte cysts, ebridians, silicoflagellates and siliceous endoskeletal dinoflagellates (e.g., actiniscidians). Radiolarians were absent in the studied interval. Of these groups, the diatom and chrysophyte cysts are the most important in core M0002A-55X; hence we indicate these data only in this paper. For each sample, at least 500 siliceous microfossils were counted using standard counting procedures [e.g., *Schrader and Gersonde*, 1978] to species level (where possible) for the diatoms. Chrysophyte cyst classification is problematic [see *Stickley et al.*, 2008]. Relative abundance (%) in this paper is quoted of a total which includes all 5 silicofossil groups encountered, unless otherwise indicated. The ratios chrysophyte cysts/(chrysophyte cysts plus diatoms) and diatoms/(diatoms plus chrysophytes) as proxies for salinity fluctuations have also been calculated.

2.4. Terrigenous Sand, Ice-Rafted Debris

[12] Evidence for fluctuations in middle Eocene ice rafting are based on 40 samples from ACEX core M0002A-55X with an average sample spacing of 13 cm (~5 ka). Samples were processed using standard methods for IRD analysis [*St. John and Krissek*, 2002; *Eldrett et al.*, 2007].

Bulk sediment samples were freeze-dried and weighed. Deionized water was added to the bulk samples and they were disaggregated in an ultrasonic bath. Dilute Calgon was added during ultrasonic disaggregation to aid in deflocculating the clays. Samples were then wet sieved at 250 μm, dried in a 60°C oven, and weighed. Visual estimates of the volume percent of the terrigenous abundance in the >250 μm fraction were made using a binocular microscope. The terrigenous grains in this sand-size fraction are considered to be ice-rafted debris.

2.5. GDGT (Glycerol Dibiphytanyl Glycerol Tetraethers) Analysis

[13] Seventeen sediment samples among those analyzed for palynology, and about 30 cm spaced, were selected for this analysis. Sediments (about 3 g dry mass) were grinded and homogenized by a grinding mill or mortar and pestle. The sediments were then extracted using Dionex™ accelerated solvent extraction (ASE 200) technique using 3 extraction cycles of dichloromethane (DCM)/methanol (2:1, v/v) at high temperature (100°C) and pressure (7.6×10^6 Pa). The extracts were separated by Al_2O_3 column chromatography using hexane/DCM (9:1, v/v) and DCM/methanol (1:1, v/v) as subsequent eluents. The polar fraction (DCM/methanol) was condensed by evaporation under a nitrogen stream, dissolved in hexane/isopropanol (99:1, v/v), ultrasonicated and filtered using a PTFE 0.4 μm filter prior to analysis by high-performance liquid chromatography/mass spectrometry (HPLC/MS). HPLC/MS analyses were performed according to *Hopmans et al.* [2000, 2004]. GDGTs were detected by single ion monitoring (SIM) of their $[M+H]^+$ ions (dwell time = 234 ms) [*Schouten et al.*, 2007] and quantified by integration of the peak areas. The tetraetherlipid index with 86 carbon atoms (TEX_{86}) was calculated according to *Schouten et al.* [2002] and converted to temperatures using the following equation [*Schouten et al.*, 2002]:

$$TEX_{86} = 0.015*T + 0.28 \quad (1)$$

[14] The branched and isoprenoid tetraether (BIT) index was calculated according to *Hopmans et al.* [2004]. Replicate analysis of samples show that the reproducibility in TEX_{86} was ~0.5°C and in BIT index ±0.01.

3. Results and Discussion

[15] Samples from core M0002A-55X, which ranges in depth between ~236 and ~241 mcd, have been analyzed for different biological, sedimentological, geochemical, and physical proxy parameters. Each proxy holds a different resolution, from centimeter scale (e.g., XRF) to decimeter scale (palynology, siliceous microfossils, IRD, TEX_{86} and BIT). Considering the age model available and the relative sedimentation rate of 24.3 m/Ma [*Backman et al.*, 2008], core M0002A-55X spans about 200,000 years between ~46 and ~46.2 Ma and the resolution achieved in this study varies between 0.5–10 ka.

[16] In the following paragraphs, we first present results obtained for the biological proxies (dinoflagellate cysts, pollen, spores, and siliceous microfossils), and assess their cyclic fluctuations and frequency. Then, we provide an explanation for such cyclic changes in the biota, giving an environmental interpretation. In this phase, we also present TEX_{86}-derived sea surface temperatures, and BIT index results. Subsequently, we integrate the signal obtained from the biological proxies with that from the sedimentological (IRD) proxy, owing the comparable spatial/temporal resolution. Finally, we integrate data to the highest-resolved geochemical XRF proxy record and we give an explanation of the significant cyclicity, associated frequency and overall environmental interpretation.

3.1. Palynology

[17] Palynomorphs are always well preserved and very abundant, reaching maximum concentrations of ~500,000/g dry sediment in two samples at 239.89 and 240.03 mcd. Pollen, dinocysts, freshwater algae, and acritarchs represent the four major palynomorph groups. Assemblages are represented for 30–80% by terrestrial palynomorphs (total pollen and spores), 3–55% by dinoflagellate cysts (Figure 2), 3–25% by acritarchs and up to 44% by freshwater algae. Angiosperm (flowering plants) pollen and spores are by far the largest group of palynomorphs. They represent 23–60% of the terrestrial palynomorphs, and their concentrations reach up to 160,000/g between 239.89 and 240.03 mcd.

[18] Terrestrial palynomorphs (pollen and spores) in marginal marine depositional environment are widely used to provide information on paleoclimate and paleoenvironment [e.g., *Hooghiemstra*, 1989; *Cheddadi and Rossignol-Strick*, 1995], including the proximity of the site to the paleoshoreline. If we assume that sea level did not undergo major continuous fluctuations over the relatively short period considered in this study [*Miller et al.*, 2005], shifts in the distance of the coring site from the paleoshoreline is negligible. Thus changes in pollen and spores can be interpreted as a proxy for paleoclimate. We consider the total terrestrial (total pollen and spores) palynomorph percentages (Figure 2) as proxy for total terrestrial organic matter input into a marine environment. The way in which pollen and spores are transported to the marine sediments is complex [*Hooghiemstra*, 1988]; however, the major modes of transport are windblown transport or transport by water currents. Pollen assemblages from nearshore sediments in arid regions are dominated by relatively few types of typical wind-transported pollen such as the bisaccate *Pinus* [*Hooghiemstra*, 1988], whereas large and thick-walled grains do not travel large distances by air [*Whitehead*, 1983]. Primarily at higher latitudes, where light is a limiting factor for plants growth, flowering plants (indicated by angiosperm pollen percentages) are favored when the growing season is longer, and possibly warmer. Gymnosperm plants (mostly producing bisaccate pollen) are more adapted to colder and drier climate.

[19] Twenty-one dinocyst genera/species were recognized. Their concentrations are always fairly high, ranging between 2,000 and 100,000 cysts/g, with peak values >170,000 between 239.89 and 240.03 mcd. *Senegalinium* and *Phthanoperidinium* are the most represented genera,

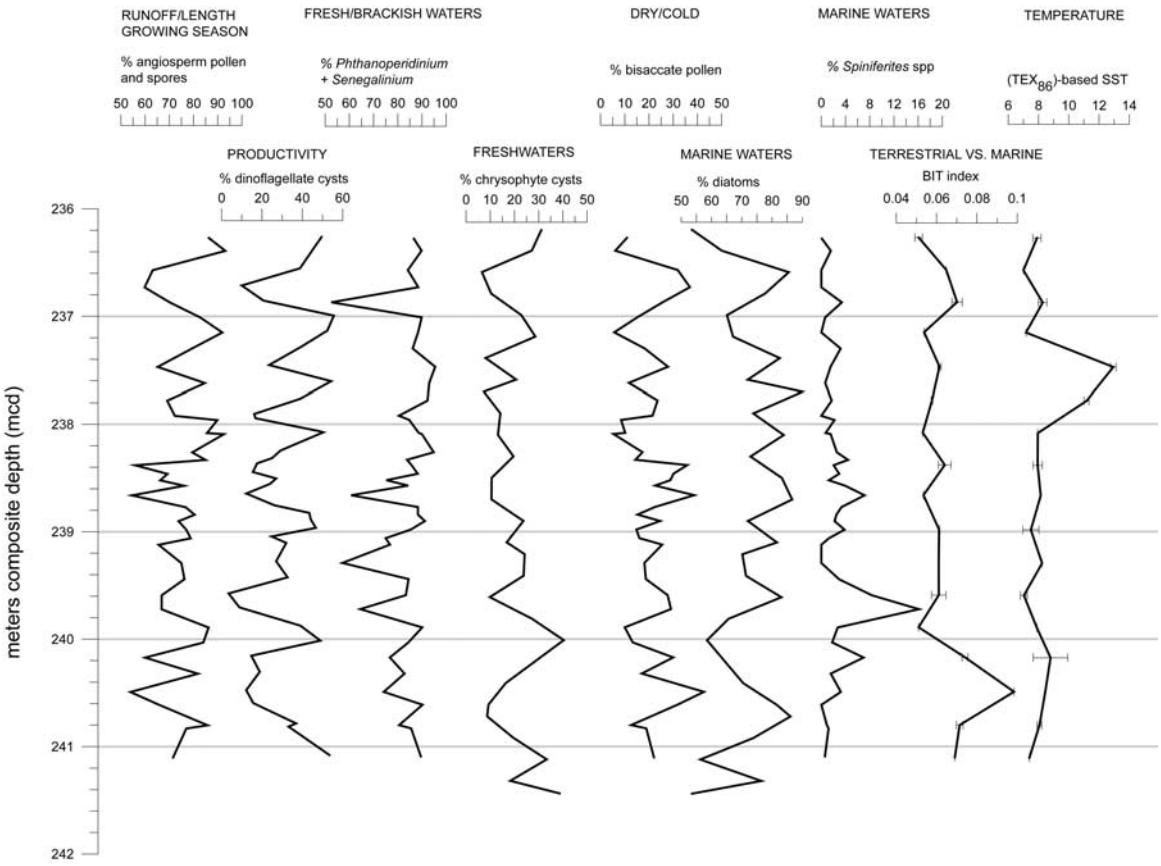

Figure 2. Main biological proxy data from ACEX core 302-2A-55X in depth domain (236–241 mcd). Angiosperm pollen plus spores and bisaccate pollen are shown as percent of total terrestrial palynomorphs; dinoflagellate cysts and terrestrial palynomorphs percentage are calculated on the total palynomorphs. *Phthanoperidinium* plus *Senegalinium* and *Spiniferites* are selected as the most indicative dinoflagellates groups and are shown as percent of total dinoflagellates cysts. Diatoms and chrysophytes are the most important siliceous microfossils in core 55X, and percentages are calculated on the total siliceous microfossils. Sea surface temperature (SSTs) derived with the paleothermometer TEX_{86} and the BIT indices are also shown.

covering 53–96% of the total dinocysts (Figure 2). *Cerodinium depressum, Cribroperidinium tenuitabulatum, Lejeunecysta* spp., *Leptodinium* sp., *Lentinia* spp, *Phelodinium* spp., *Selenopemphix* spp. and *Spiniferites* spp. are among the other well represented dinocysts in the assemblages. The *Spiniferites* group reaches up to 16% of the total dinocysts (Figure 2). Detailed palynological data, which are not presented here, can be obtained upon request to the corresponding author. The dinocyst assemblages are dominated by the brackish to freshwater tolerant genera *Senegalinium* and *Phthanoperidinium* [e.g., *Brinkhuis*, 1994; *Sluijs et al.*, 2003, 2005], which percentages are thus used as indicators of freshwater influence. Lower percentages of these genera indeed usually correspond to higher percentages of cysts of *Spiniferites* (Figure 2), which includes species with preference for open marine waters [e.g., *Marret and Zonneveld*, 2003 and references therein].

[20] Dinocysts recovered in core M0002A-55X are dominated (70–100%) by species with peridinoid affinity. As most (extant) peridinoids are heterotrophs, higher dinocyst percentages in our record may suggest higher primary productivity (see discussion of *Sluijs et al.* [2005] and references therein).

3.2. TEX_{86} and BIT Index

[21] Sea surface temperatures (SSTs) reconstructed using the TEX_{86} paleothermometer [*Schouten et al.*, 2002] show fairly stable values around 8°C in 15 of the 17 samples analyzed (Figure 2). Only two samples, at 237.47 and 237.78 mcd record values significantly higher (11.3°C and 13.1°C, respectively).

[22] The BIT index, a proxy for the relative contribution of soil organic matter relative to marine organic matter [*Hopmans et al.*, 2004], shows always low values (<0.1),

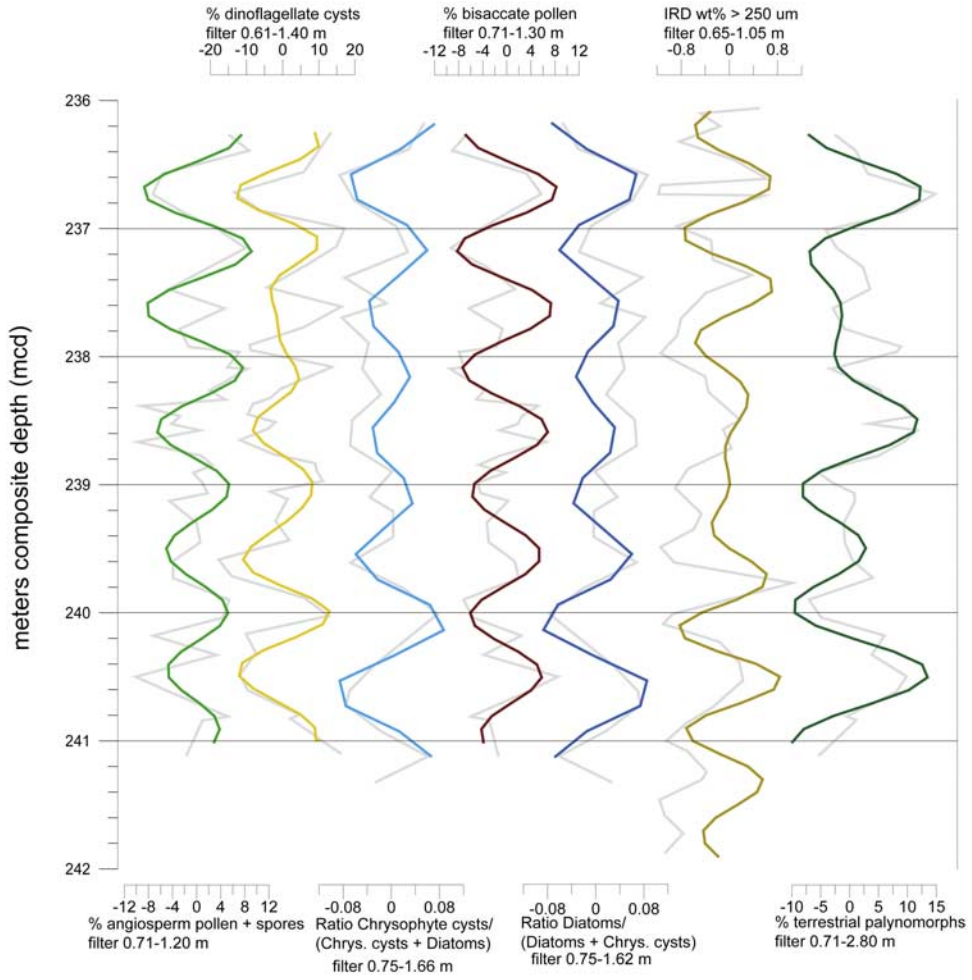

Figure 3. Gaussian band-pass filter on palynomorphs (angiosperm pollen and spores, dinoflagellates cysts, bisaccate pollen, terrestrial palynomorphs), siliceous microfossils (chrysophyte cysts and diatoms), and IRD records, showing their significant periodicity. Blackman-Tuckey power spectral analysis was performed with the AnalySeries Program version 1.1.1 [*Paillard et al.*, 1996] on records in depth domain using a Bartlett window and confidence interval set at 90%. Before spectral analysis, proxy records were detrended and normalized to unit variance. Gaussian band-pass filtering was subsequently applied for significant peaks in the power spectra (compare Figure 4).

with the highest value (0.09) at 240.49 mcd. Sampling resolution is not sufficient to highlight possible cyclical fluctuations in SST (TEX_{86}) and BIT index. Therefore these two proxies will not be discussed further. However, the BIT index seems to mirror the terrestrial palynomorph percentages trend (Figure 2).

3.3. Siliceous Microfossils

[23] Siliceous microfossils (silicofossils) are very abundant throughout the biosiliceous ooze (unit 2) with core M0002A-55X representing the highest silicofossil levels of the entire biosiliceous interval recovered during ACEX drilling (between 0.7 and 6.9 $\times$ 10^8 silicofossils/g) [*Stickley et al.*, 2008]. Diatoms and chrysophyte cysts are the two main silicofossil groups encountered in this core, with diatoms being the most important group (55–90% of silicofossils, Figure 2). All diatom taxa are considered to be neritic marine to brackish tolerant. A significant number of these are heavily silicified resting spores, which on account of their high abundance, good preservation and association with other shallow water microfossils are considered in situ. Curious needle-like diatoms are also abundant in core M0002A-55X (11–71% of total diatoms) often pseudomatted, which may indicate periodic intensified stratification [see *St. John*, 2008]. Chrysophyte cysts represent the resting stage of freshwater algae, assumed living in situ in the periodically fresh surface waters of the Arctic Ocean throughout most of the biosiliceous interval in ACEX sediments, except perhaps for periods where in situ cysts and those transported via river runoff may be encountered (see *Stickley et al.* [2008] for discussion). Whether or not chrysophytes are transported or in situ is not important here, as either interpretation would suggest a freshening of the surface waters at the Lomonosov Ridge when they are

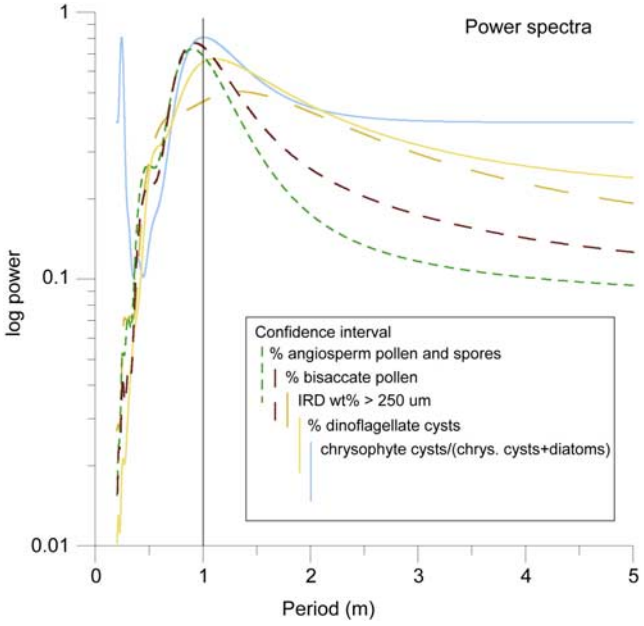

Figure 4. Power spectra shown for selected proxy records (see Figure 3). All the spectra displayed show a significant periodicity of about 1 m.

abundant. Chrysophyte cysts represent 7–40% of total silicofossils within core M0002A-55X (Figure 2).

[24] A chrysophytes/(chrysophytes plus diatoms) ratio (C/C+D) is calculated (Figure 3) to stress the relative contribution of chrysophyte cysts versus diatoms (the two main silicofossil groups). As chrysophyte cysts indicate fresh surface water, the higher the ratio, the greater the freshwater influence. The complementary ratio (D/C+D) is also shown (Figure 3) to facilitate the discussion. It is interpreted as indicative of relatively higher marine water influence.

3.4. Cycles in the Biological Proxies: Frequency and Environmental Interpretation

[25] The statistical analysis performed with AnalySeries version 1.1.1 [*Paillard et al.*, 1996] on some of the most representative biological proxy record in a depth domain indicates a significant 1 m cycle in several proxies (Figures 3 and 4). Considering the sedimentation rate derived for this section of the ACEX core (~24.3 m/Ma) [*Backman et al.*, 2008], 1 m corresponds to ~41 ka, suggesting obliquity-paced biotic changes. There is a clear correlation (Figure 3) between (1) total terrestrial palynomorphs percentages, bisaccate pollen percentages, and diatom ratio (diatoms/chrysophyte cysts plus diatoms) and (2) angiosperm pollen and spore percentages, dinocysts percentages, and chrysophyte cysts ratio chrysophyte cysts/chrysophyte cysts plus diatoms).

[26] This overall correlation allows us to translate fluctuations of these two major groups into environmental signals, although biological proxies are more dependent than other proxies on a complex variety of environmental variables.

[27] When total terrestrial palynomorph percentages are higher, bisaccate pollen percentages are higher, and angiosperm pollen and spores percentages are lower (Figure 3 and Table 1). This implies that total terrestrial palynomorphs (total pollen and spores) do not indicate terrestrial river-transported input, but likely other types of input (e.g., wind). Higher total terrestrial palynomorphs (and bisaccate) thus indicate phases of drier, possibly colder conditions (shorter blooming season) on land, as bisaccate are mostly windblown into a marine environment [e.g., *Hooghiemstra*, 1988].

[28] Accordingly, in the marine environment, higher terrestrial palynomorphs correspond to relatively lower dinocysts, lower chrysophyte cysts (C/C+D) and higher diatom (D/C+D) ratios. Dinocyst assemblages are dominated by peridinoids (heterotrophs) and mainly are composed of *Senegalinium* spp. and *Phthanoperidinium* spp., which include freshwater and brackish water tolerant species [e.g., *Brinkhuis*, 1994; *Sluijs et al.*, 2003, 2005]. Hence periods with low dinocyst percentages indicate lower productivity possibly related to lower runoff, which correlate to drier conditions on land as suggested by pollen. Lower runoff and/or decreased stratification are also confirmed by lower chrysophyte cysts (C/C+D) ratios. Higher diatom ratios (D/C+D) represent higher salinity, more marine conditions, less stratification. Higher diatom percentages often correspond to higher *Spiniferites* cyst percentages (Figure 2), both indicating a stronger marine influence (higher salinity) in the Arctic Ocean.

[29] These obliquity-paced environmental changes are compatible with changes in seasonality. When obliquity is reduced, summers are relatively shorter. In an obliquity minimum configuration higher total terrestrial palynomorphs due to higher bisaccate pollen is the prevailing vegetation-derived signal. Drier and possibly colder conditions on land are testified to by higher wind-transported bisaccate pollen. Shorter summers imply longer periods of darkness and shorter blooming season, relatively reducing the percentages of flowering plants/angiosperm pollen in our record. In this configuration runoff also decreases, the nutrient input by runoff into the Arctic Ocean is lower, and productivity and stratification are reduced (lower dinocysts and lower chrysophyte cysts). The Arctic Ocean is thus

Table 1. Selected Biological Proxies and Their Environmental Interpretation

Proxy	Trend	Environmental Interpretation
Percent angiosperm pollen and spores	low	short growing season, low freshwater input, low humidity
Percent dinoflagellate cysts	low	low productivity, low freshwater influence
Chrysophyte cysts ratio (C/C+D)	low	low freshwater input, low stratification
Percent bisaccate pollen	high	cold and dry on land
Percent terrestrial palynomorphs (total pollen and spores)	high	high terrestrial input
Diatom ratio (D/C+D)	high	higher salinity, marine conditions, low stratification

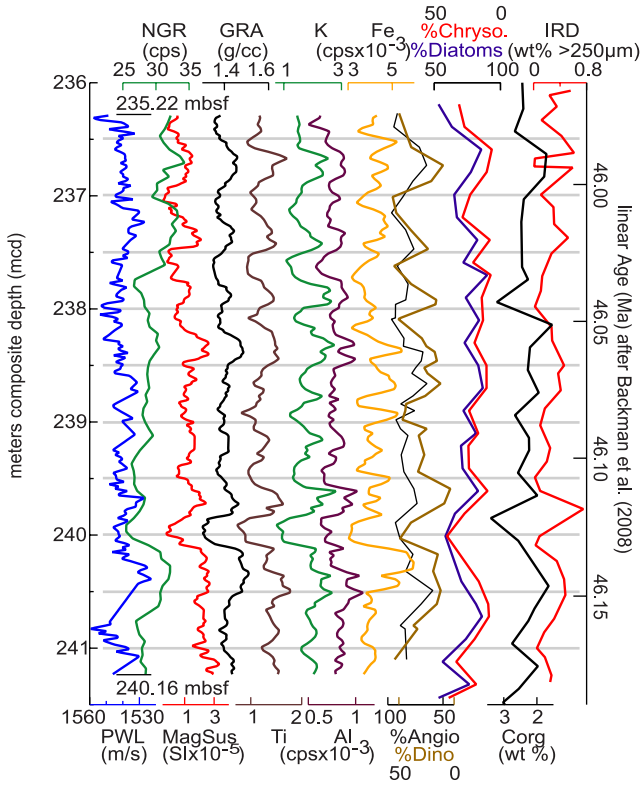

Figure 5. Physical and biological proxy data from ACEX core 302-2A-55X (235–240.41 m below seafloor and 236.07–241.48 mcd). Shown are *P* wave velocity (PWL), natural gamma counts (NGR), magnetic susceptibility (MagSus), bulk density (GRA), XRF-derived elemental counts of titanium (Ti), potassium (K), aluminum (Al), and iron (Fe), relative abundances of angiosperms (Angio), dinocysts (Dino), chrysophytes (Chryso), and diatoms, organic carbon by weight percent (C_{org} [from *Stein et al.*, 2006]), and terrigenous sediment weight percent >250 μm (IRD). Meters composite depth (mcd) is annotated on the left vertical axis, while ages derived from a simple linear age model [*Backman et al.*, 2008] appear along the right. Horizontal grey lines mark 50 cm depth intervals. Note apparent 50 cm wavelength cyclicity in MagSus, GRA, Ti, K, and Al.

relatively more influenced by marine waters, which are represented by relatively higher amount of diatoms (D/C+D) and cysts of *Spiniferites.*

3.5. Terrigenous Sand and Ice-Rafted Debris (IRD)

[30] Terrigenous sand abundances in the >250 μm fraction fluctuate between 0 and 0.8 wt % in core M0002A-55X (Figures 3 and 5), which are comparable to Plio-Pleistocene abundances in the central Arctic [*St. John*, 2008] and interglacial late Pleistocene abundances across the Arctic [*Darby et al.*, 2006]. Similarly timed but greater amplitude fluctuations are also observed in the 150–250 μm terrigenous sand fraction [*St. John*, 2008]. High weight percents (and derived high IRD mass accumulation rates [*St. John*, 2008]) are evidence for the earliest Cenozoic ice presence in the Northern Hemisphere, beginning at ~46.2 Ma.

[31] Concurrent with the initial ice rafting is an increase in the abundance of needle-like diatoms [*Stickley et al.*, 2008]. In addition, salinity reconstructions from fish bone carbonate show a positive excursion from between 21–25 ppt to 27 ppt close to the time of core M0002A-55X deposition (in core 2A 56X [*Waddell and Moore*, 2008]). Taken together, this evidence supports the formation of sea ice in the middle Eocene as indicated by mechanical surface texture feature on quartz grains from this interval and IRD weight percents (>1 wt % [*St. John*, 2008, Figures 2 and 3]) that are on the order of those in Pleistocene glacial stages in the Arctic [*Darby et al.*, 2006]. Thus high inputs of IRD in the middle Eocene likely reflect a combination of increased sea ice, as well as the presence of glacial ice and the subsequent calving of icebergs from the Arctic Ocean margin. Increased IRD abundances correspond to higher total terrestrial palynomorphs percentages, bisaccate pollen percentages, and diatom ratio (diatoms/chrysophyte cysts plus diatoms) (Figure 3).

[32] Cycles of sea ice and glacial ice formation might have been facilitated by the spring/summer melt after colder winter temperatures and/or longer dark winter seasons. A larger-scale control of the initial onset of Arctic ice may be the drawdown in atmospheric pCO_2 between ~46 and 43 Ma [*Pearson and Palmer*, 2000; *Lowenstein and Demicco*, 2006] enabling the nucleation of small glaciers on land and partial freezing of the surface Arctic Ocean, especially during times of low insolation.

3.6. X-ray Fluorescence (XRF)

[33] A cyclostratigraphic analysis of data sets usually requires continuous long and high-resolution records, with additional good age control by biostratigraphic or magnetostratigraphic data. In the case of the ACEX record, these requirements are only partially met, as stratigraphic sections below the top few tens of meters are not fully recovered, and age control is mostly provided by biostratigraphic means only [*Backman et al.*, 2008]. Nevertheless, it has proved possible to extract information from the cyclical nature that several physical and biological proxies provide.

3.6.1. Proxy Relationships

[34] Visual inspection of the physical proxy parameters shown in Figure 5 indicates a positive correlation between bulk density (GRA), magnetic susceptibility (MagSus), natural gamma counts (NGR), XRF-derived counts of potassium (K), aluminum (Al), titanium (Ti), and to some extend the weight percent abundance of the >250μm terrigenous sediment (IRD), while the bulk *P* wave sound velocity (PWL), bulk organic carbon (C_{org}) [from *Stein et al.*, 2006] are anticorrelated.

[35] With respect to the bulk density (GRA) and correlated parameters, the biological proxies of chrysophyte cysts, angiosperm pollen and spores and dinocyst abundance are negatively correlated, while diatom abundance is positively correlated on length scales of decimeters to meters. There are several physical proxy parameters that do not show a strong correlation with other parameters,

notably XRF iron counts (Fe), and silica (not shown here). For Fe, this lack of strong correlation can be explained by the observation of very high pyrite content in this core, which at least partially reflects remobilization of iron. XRF-derived silica counts will reflect both biogenic (e.g., diatoms) as well as nonbiogenic terrigenous components, and would therefore also be expected to show a different and more complicated relationship with other proxy parameters.

[36] We interpret these relationships such that higher values of the parameters GRA, MagSus, and NGR indicate an enhanced terrigenous component, also reflected in elevated XRF-derived Fe, K, Ti and Al counts, while corresponding lower *P* wave velocities might be due to the lower bulk modulus of sediment in the absence of the structural interlocking framework provided by diatoms. During times of higher terrigenous input, the TOC content is lower. Higher terrigenous input also corresponds to smaller contributions by angiosperm pollen and spores, dinocysts and chrysophytes (lower productivity, shorter blooming season), but higher contributions by bisaccate pollen and diatoms (drier conditions on land, more marine conditions). Higher input of terrigenous material and IRD might have been facilitated by colder temperatures, drier conditions and/or longer dark winter seasons increasing sea ice transport of material, and also affecting surface ocean productivity and food availability. Diatom abundance may follow that for IRD because they bloom and are deposited in spring/summer when IRD are present and deposited. At present, ice-associated phytoplankton blooms in the Bering Sea are modulated by seasonal sea ice cover. During cold years, the main bloom occurred in spring along the ice edge, while during the warmer years blooms occur in later (May or June) in relatively warmer waters [*Jin et al.*, 2007, and references therein]. This may have also been the case if sea ice was present in the middle Eocene, although making assumptions about sea ice–related diatoms for the pre-Quaternary is problematic and speculative.

3.6.2. Signal Analysis

[37] In order to establish the presence, nature and variability of cyclical signals within the proxy data sets, it is valuable to consider multiple proxies simultaneously, such that the signal component common to all can be separated from noise that is invariably contained within these short data sets. In order to do so we have applied an approach previously developed for meteorological data sets, namely the singular spectral analysis (SSA) decomposition [*Vautard and Ghil*, 1989; *Vautard et al.*, 1992), here extended to multiple proxy channels (MSSA) [*Plaut and Vautard*, 1994; *Jiang et al.*, 1995]. This approach makes it possible, without a priori knowledge, (1) to extract those oscillations that are common to all proxy series considered, (2) to establish what the dominant periodicities are, and (3) to reconstruct the higher-order principal components thus extracting signal from a noisy background.

[38] We ran several experiments using the MSSA approach to first identify those components that show correlated oscillations (shown in Figure 5, with Fe added). Results indicate that XRF-derived K, Al, Ti correlate strongly, while both Si and Fe show oscillations that are not common to other physical property parameters such as GRA bulk density. The MSSA decomposition of a subset of our proxy curves (GRA, Ti, K) is shown in Figure 6, using a total of eight proxy channels as input to the analysis (GRA, NGR, PWL, MagSus, XRF K, Al, Ti, Fe). This method allows the identification of a set of strong oscillations that are common to these parameters shown in Figure 5, and represented by paired principal components 1–8, 11–14, 16 and 17. Figure 7 shows a maximum entropy [*Press et al.*, 1992] spectral analysis for these significant principal component oscillations, together with their respective ordered eigenvalues.

[39] Principal components are sorted in order of how much variance of the record they explain. The top 8 most significant principal components confirm the visually apparent cyclicity with periods of about 50 and 100 cm (Figure 5). These frequency components are compatible with a Milankovitch type orbital forcing, if converting cycles per meter to cycles per million years using the simple linear age model from *Backman et al.* [2008]. The fully reconstructed MSSA channels from our analysis are shown in Figure 8, which also shows the combined extracted signal from all eight proxies, but excluding Fe, and reversing the sign of PWL.

3.6.3. Orbital Analysis

[40] Having established that the oscillations extracted from our data sets are compatible with an orbital forcing, we generated a relative floating age scale by matching maxima in IRD with minima in insolation at the Sites latitude of about 85°N during June and July (Figure 9). The approach results in fairly stable and linear sedimentation rates of ~25 m/Ma, compatible with the biostratigraphically derived values of *Backman et al.* [2008].

[41] We note that our data sets record variability at the obliquity and climatic precession frequencies that dominate insolation quantities, and are thus seasonal signals. Purely annual average variations in insolation would consist of eccentricity contributions only. At present it is not possible to establish a difference between terrigenous and biological proxies in terms of main forcing frequencies, as both were sampled at different resolutions. However, at first sight (Figure 5) it appears that the biological proxies show a stronger response to forcing at the longer obliquity period, which, if confirmed, could be explained by a stronger response of fauna and flora to seasonal darkness. Contrarily, the terrigenous components, which are conceivably directly driven by sea ice and/or glacial ice formation and extent, can be expected to correspond more directly to seasonal insolation.

4. Conclusions

[42] Continuous X-ray fluorescence (XRF) scanning of middle Eocene (~46 Ma) ACEX core M0002A-55X revealed a strong cyclical signal in some major and trace geochemical elements (e.g., Fe, K, Ti, Al, Si) (Figure 8). XRF and physical properties (GRA, MagSus, PWL, and NGR) analysis has evidenced cyclicities with periods of about 50 cm and 100 cm (Figure 5). Using the age model of *Backman et al.* [2008] and the derived sedimentation rate of 24.3 m/Ma, these frequency components are compatible

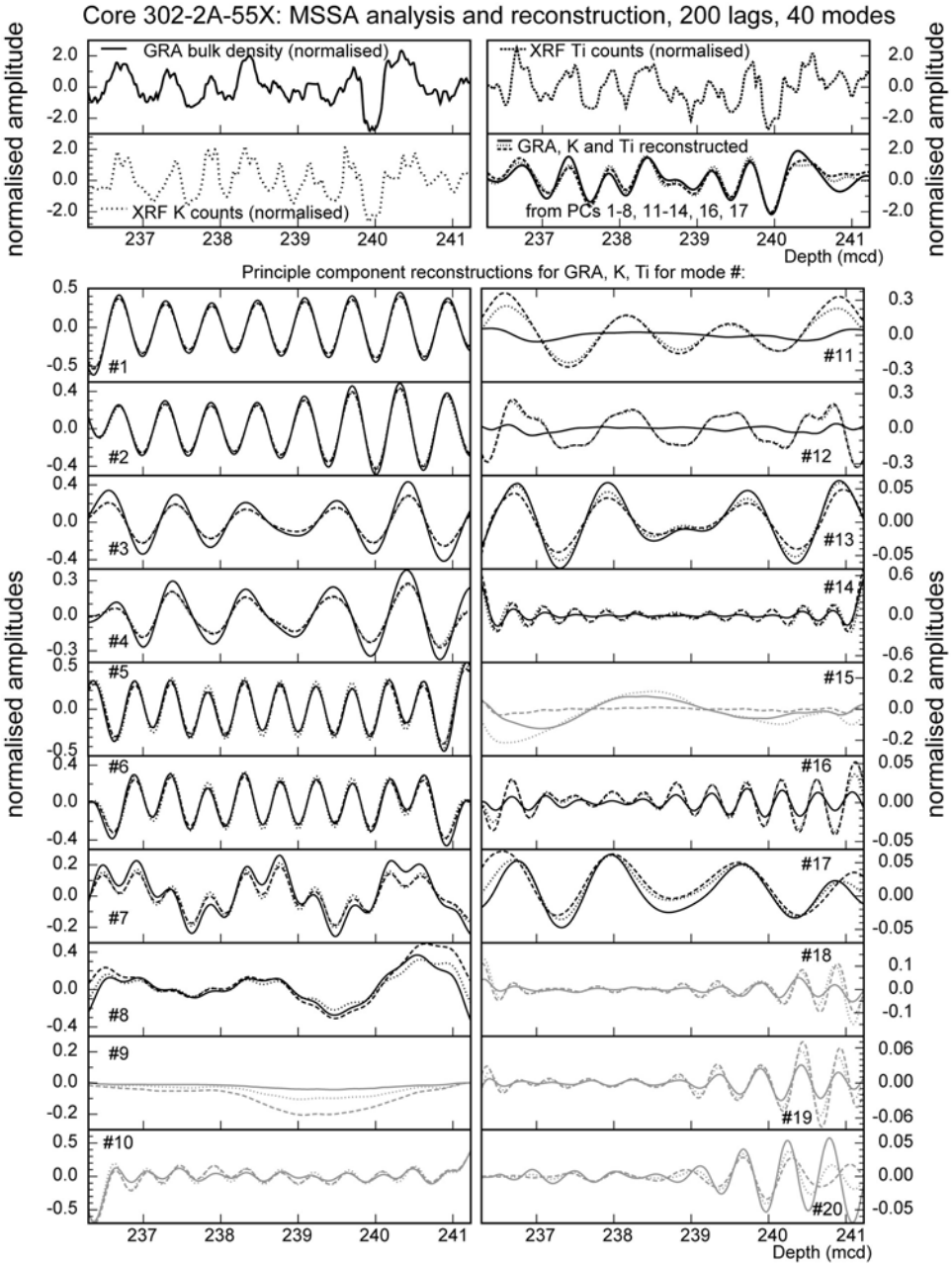

Figure 6. Multichannel singular spectral analysis decomposition and reconstruction of eight parameters GRA, MagSus, PWL, NGR, and XRF K, Ti, Al, and Fe counts, using 200 1 cm lags and 40 modes. (top) Three of the eight-channel inputs (GRA, K, and Ti), all linearly detrended and divided by their standard deviation (normalized), as well as their reconstructions using principal component decompositions 1–8, 11–14, 16, and 17. (bottom) First 20 out of 40 principle component reconstructions for GRA and XRF K and Ti. Those used for reconstruction are shown in black; others are shown as shaded. Several cyclicities are apparent and can be quantified (see Figure 7).

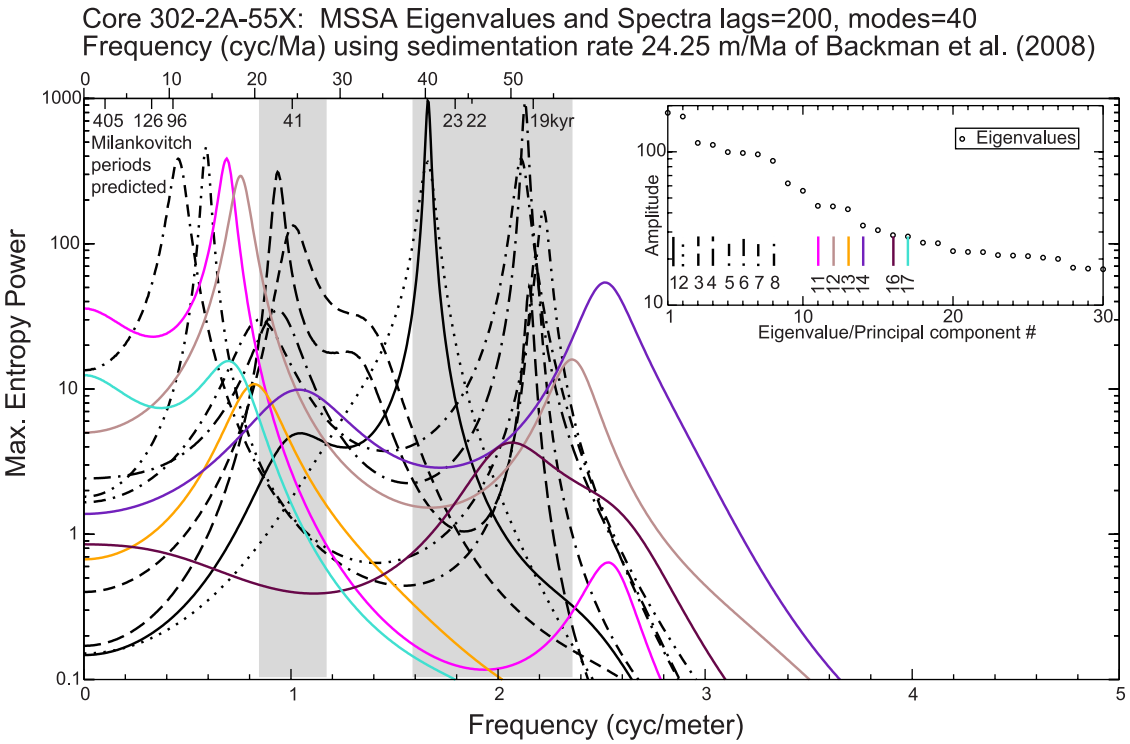

Figure 7. Maximum entropy spectra [*Press et al.*, 1992] calculated for principal component reconstructions shown in Figure 6. Each spectral line corresponds to one of the bottom plots in Figure 6. (inset) Ordered by amplitude, the eigenvalue of the first 30 principal components, providing the key for individual spectra in the larger plot. Lower horizontal axis provides frequency in cycles per meter. This is converted to equivalent cycles per million years by using the simple linear age model provided by *Backman et al.* [2008] and shown in top horizontal axis. Also shown are predicted periods of Milankovitch orbital cycles [*Laskar et al.*, 2004]. Principal periodicities identified cluster around 1.6–2.4 cycles/m and 0.6–1.3 cycles/m. Vertical shaded bars indicate the frequency range of components 1–8 with the highest eigenvalues.

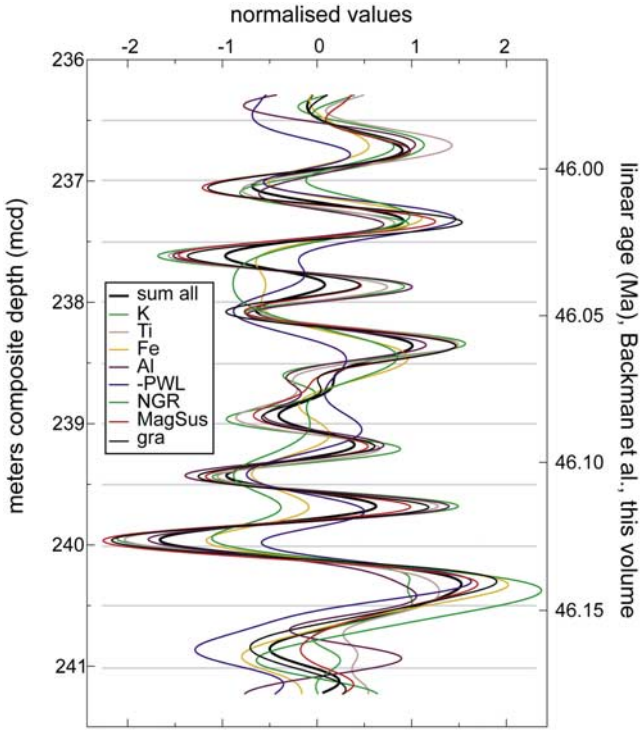

Figure 8. Reconstructed and combined principle components identified in Figure 6. Note reversed scale for sound velocity (PWL). Also shown is the average of all reconstructed curves (sum all, thicker black line), which represents that part of the signal that is common to all eight proxies used (GRA, NGR, PWL, MagSus, XRF, K, Ti, and Al). Note that iron (Fe) is the one element that does not confirm to the cyclicity expressed by the other proxies and is excluded from sum.

with a Milankovitch type orbital forcing, with the oscillations at 50 cm and at 100 cm representing precession and obliquity, respectively. The longer 100 cm cyclicity is also present in the biological (pollen, dinocysts, and siliceous microfossils) proxies and in the sedimentological (IRD) proxy (Figures 3 and 5).

[43] Concerning the environmental changes associated with the cycles, higher values of the parameters GRA, MagSus, and NGR indicate an enhanced terrigenous input, also reflected in elevated XRF-derived Fe, K, Ti and Al counts. A higher terrigenous component corresponds to lower organic carbon concentration, to relatively smaller contributions by angiosperm pollen and spores, dinocysts and chrysophyte cysts (lower productivity, shorter growing season for flowering plants), but higher contributions by bisaccate pollen and diatoms (drier conditions on land, more marine conditions), and higher IRD (Figure 3). Our interpretation is that these changes correspond to an obliquity minimum configuration. Higher input of terrigenous material and IRD can be indeed facilitated by colder temperatures, drier conditions and/or longer dark winter (shorter summer) seasons increasing sea ice transport of material, and also affecting surface ocean productivity and food availability. Diatom abundance may follow IRD trends because they bloom in spring/summer when IRD are deposited.

[44] The sample resolution for the biological proxy records could be sometimes at the limit at what would resolve climatic precession driven cycles with statistical confidence (ca 50 cm spacing), using the age model of *Backman et al.* [2008]. Out of the biological proxies, only the diatom abundance appears to show cyclicity with a component around 50 cm. However, the lack of significant 50 cm cycles for the biological proxies could also mean that plants and phytoplankton respond stronger to seasonal darkness, whereas the terrigenous components, directly driven by sea ice and/or glacial ice formation and extent, respond more directly to seasonal insolation.

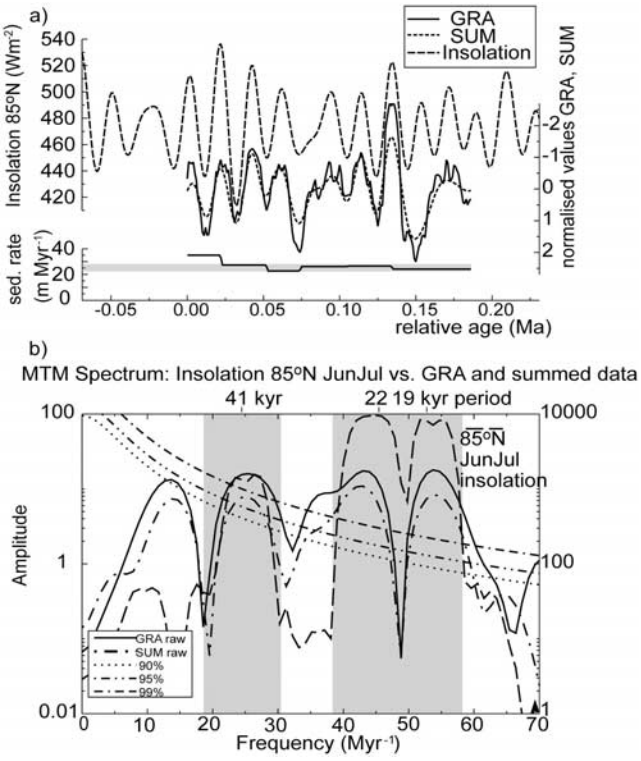

Figure 9. (a) Nominal tuning of extracted proxy signal to 85°N June-July summer insolation [*Laskar et al.*, 2004]. Shown are insolation and GRA (bulk density) and sum (sum of recombined principal components) (sum, Figure 8), both normalized. Maximum SUM and GRA values were adjusted to minimum insolation values. Data are plotted against a relative age scale starting at the top of the data set, but insolation on this plot corresponds to the interval 45.96–46.2 Ma using the solution from *Laskar et al.* [2004]. Also shown is the implied sedimentation rate. Median values are around 25 m/Ma, very close to those obtained by *Backman et al.* [2008]. (b) Spectra of data in Figure 9a, using the multitaper method of *Thomson* [1982], together with autoregressive model of order 1 background noise models at 90, 95, and 99% significance.

[45] **Acknowledgments.** This research used samples and data provided by the Integrated Ocean Drilling Program (IODP). F.S. and E.v.S. acknowledge Hemmo Abels for discussion on the spectral analysis and Timme Donders for discussion on vegetation dynamics and the two reviewers Bridget Wade and Luigi Jovane. Gert-Jan Reichart, Ellen Hopmans, Cornelia Blaga, and Elisabeth van Bentum are thanked for analytical assistance. We thank Walter Hale (IODP Bremen core repository) for core handling. We acknowledge NWO (Netherlands Organization for Scientific Research) for funding, VISTA (Norwegian Academy of Science and Letters and Statoil) Project 6248, and the Research Council of Norway (RCN). This is NSG publication 20080102.

References

Aagaard, K., and E. C. Carmack (1989), The role of sea ice and other waters in the Arctic circulation, *J. Geophys. Res.*, *94*(C10), 485–498.

Backman, J., et al. (2008), Age model and core-seismic integration for the Cenozoic Arctic Coring Expedition sediments from the Lomonosov Ridge, *Paleoceanography*, doi:10.1029/2007PA001476, in press.

Battarbee, R. W., and M. J. Kneen (1982), The use of electronically counted microspheres in absolute diatom analysis, *Limnol. Oceanogr.*, *27*, 184–188.

Battarbee, R. W., L. Carvalho, V. J. Jones, R. J. Flower, N. G. Cameron, H. Bennion, S. Juggins (2001), Diatoms, in *Tracking Environmental Change Using Lake Sediments*, vol. 3, *Terrestrial, Algal, and Siliceous Indicators*, edited by J. P. Smol, W. Last, and H. J. B. Birks, pp. 155–202, Kluwer Acad., Norwell, Mass.

Brinkhuis, H. (1994), Late Eocene to early Oligocene dinoflagellate cysts from the Priabonian type-area (northeast Italy): Biostratigraphy and palaeoenvironmental interpretation, *Palaeogeogr. Palaeoclimatol. Palaeoecol.*, *107*, 121–163.

Brinkhuis, H., et al. (2006), Episodic fresh surface water in the Eocene Arctic Ocean, *Nature*, *441*, 606–609.

Cheddadi, R., and M. Rossignol-Strick (1995), Eastern Mediterranean quaternary paleoclimates from pollen and isotope records of marine cores in the Nile cone area, *Paleoceanography*, *10*, 291–300.

Darby, D. A., L. Polyak, and H. A. Bauch (2006), Past glacial and interglacial conditions in the Arctic Ocean and marginal seas—A review, *Prog. Oceanogr.*, *71*, 129–144.

Eldrett, J. S., I. C. Harding, P. A. Wilson, E. Butler, and A.P. Roberts (2007), Continental ice in Greenland during the Eocene and the Oligocene, *Nature*, *446*, 176–179.

Expedition 302 Scientists (2006), Sites M0001–M0004, in *Arctic Coring Expedition (ACEX)*, *Proc. Integr. Ocean Drill. Program, 302*, doi:10.2204/iodp.proc.302.104.2006.

Fensome, R. A., and G. L. Williams (2004), *The Lentin and Williams Index of Fossil Dinoflagellates 2004 Edition*, 909 pp., Am. Assoc. of Stratigr. Palynol. Found., College Station, Tex.

Greenwood, D. R., and S. L. Wing (1995), Eocene continental climates and latitudinal temperature gradients, *Geology*, *23*, 1044–1048.

Hays, J. D., J. Imbrie, and N. J. Shackleton (1976), Variations in the Earth's orbit: Pacemaker of the ice ages, *Science*, *194*, 1121–1132.

Hooghiemstra, H. (1988), Palynological records from northwest African marine sediments: A general outline of the interpretation of the pollen signal, *Philos. Trans. R. Soc. London, Ser. B*, *318*(1191), 431–449.

Hooghiemstra, H. (1989), Variations of the NW African trade wind regime during the last 140000 years: Changes in pollen evidenced by marine sediment records, in *Paleoclimatology and Paleometeorology: Modern and Past Patterns of Global Atmospheric Transport*, edited by M. Leinen and M. Sartnthein, pp. 733–770, Kluwer Acad., Norwell, Mass.

Hopmans, E. C., S. Schouten, R. D. Pancost, M. J. T. van der Meer, and J. S. Sinninghe Damsté (2000), Analysis of intact tetraether lipids in archaeal cell material and sediments using high performance liquid chromatography/atmospheric pressure ionization mass spectrometry, *Mass Spectrom.*, *14*, 585–589.

Hopmans, E. C., J. W. H. Weijers, E. Schefuß, L. Herfort, J. S. Sinninghe Damsté, and S. Schouten (2004), A novel proxy for terrestrial organic matter in sediments based on branched and isoprenoid tetraether lipids, *Earth Planet. Sci. Lett.*, *224*, 107–116.

Jackson, C. S., and A. J. Broccoli (2003), Orbital forcing of Arctic climate: Mechanisms of climate response and implication for continental glaciation, *Clim. Dyn.*, *21*, 539–557.

Jahren, A. H., and L. S. L. Sternberg (2003), Humidity estimate for the middle Eocene Arctic rain forest, *Geology*, *31*, 463–466.

Jakobsson, M., et al. (2007), The Early Miocene onset of a ventilated circulation regime in the Arctic Ocean, *Nature*, *447*, 986–990.

Jansen, J. H. F., S. J. Van der Gaast, B. Koster, and A. J. Vaars (1998), CORTEX, a shipboard XRF-scanner for element analyses in split sediment cores, *Mar. Geol.*, *151*, 143–153.

Jiang, N., D. Neelin, and M. Ghil (1995), Quasi-quadrennial and quasi-biennial variability in the equatorial Pacific, *Clim. Dyn.*, *12*, 101–112.

Jin, M., C. Deal, J. Wang, V. Alexander, R. Gradinger, S. Saitoh, T. Iida, Z. Wan, and P. Stabeno (2007), Ice-associated phytoplankton blooms in the southeastern Bering Sea, *Geophys. Res. Lett.*, *34*, L06612, doi:10.1029/2006GL028849.

Lammers, R. B., A. I. Shiklomanov, C. J. Vorosmarty, B. M. Fekete, and B. J. Peterson (2001), Assessment of contemporary Arctic river runoff based on observational discharge records, *J. Geophys. Res.*, *106*, 3321–3334.

Laskar, J., P. Robutel, F. Joutel, M. Gastineau, A. C. M. Correia, and B. Levrard (2004), A long-term numerical solution for the insolation quantities of the Earth, *Astron. Astrophys.*, *428*, 261–285.

Lowenstein, T. K., and R. V. Demicco (2006), Elevated Eocene atmospheric CO_2 and its subsequent decline, *Science*, *313*, 1928.

Marret, F., and K. F. Zonneveld (2003), Atlas of modern organic-walled dinoflagellate cyst distribution, *Rev. Palaeobot. Palynol.*, *125*, 1–200.

Meincke, J., B. Rudels, and H. J. Friedrich (1997), The Arctic Ocean-Nordic Sea thermohaline system, *ICES J. Mar. Sci.*, *54*, 283–299.

Miller, K. G., M. A. Kominz, J. V. Browning, J. D. Wright, G. S. Mountain, M. E. Katz, P. J. Sugarman, B. S. Cramer, N. Christie-Blick, and S. F. Pekar (2005), The Phanerozoic record of global sea-level change, *Science*, *310*, 1293–1998.

Moran, K., et al. (2006), The Cenozoic palaeoenvironment of the Arctic Ocean, *Nature*, *441*, 601–605.

Paillard, D., L. Labeyrie, and P. Yiou (1996), Macintosh program performs time-series analysis, *Eos Trans. AGU*, *77*(39), 379.

Pearson, P. N., and M. R. Palmer (2000), Atmospheric carbon dioxide concentrations over the past 60 million years, *Nature*, *406*, 695–699.

Pearson, P. N., B. E. van Dongen, C. J. Nicholas, R. D. Pancost, S. Schouten, J. M. Singano, and B. S. Wade (2007), Stable warm tropical climate through the Eocene epoch, *Geology*, *35*, 211–214.

Plaut, G., and R. Vautard (1994), Spells of low-frequency oscillations and weather regimes in the Northern Hemisphere, *J. Atmos. Sci.*, *51*, 210–236.

Press, W. H., S. A. Teukolsky, W. T. Vetterling, B. P. Flannery (1992), *Numerical Recipes: The Art of Scientific Computing*, 2nd ed., Cambridge Univ. Press, New York.

Sangiorgi, F., H. J. Brumsack, D. A. Willard, H. Brinkhuis, S. Schouten, C. E. Stickley, M. O'Regan, G.-J. Reichart, and J. S. Sinninghe Damsté (2008), A 26 million years gap in the central Arctic record at the greenhouse-icehouse transition: Looking for clues, *Paleoceanography*, *23*, PA1S04, doi:10.1029/2007PA001477.

Schouten, S., E. C. Hopmans, E. Schefuß, and J. S. Sinninghe Damsté (2002), Distributional variations in marine crenarchaeotal membrane lipids: A new organic proxy for reconstructing ancient sea water temperatures?, *Earth Planet. Sci. Lett.*, *204*, 265–274.

Schouten, S., C. Huguet, E. C. Hopmans, and J. S. Sinninghe Damsté (2007), Improved analytical methodology of the TEX_{86} paleothermometry by high-performance liquid chromatography/atmospheric pressure chemical ionization-mass spectrometry, *Anal. Chem.*, *79*, 2940–2944.

Schrader, H. J., and R. Gersonde (1978), Diatoms and silicoflagellates, in *Micropaleontological Counting Methods and Techniques: An Exercise of an Eight Metres Section of the Lower Pliocene of Cap Rossello, Sicily*, edited by W. J. Zachariasse et al., *Utrecht Micropaleontol. Bull.*, *17*, 129–176.

Serreze, M. C., A. P. Barrett, A. G. Slater, R. A. Woodgate, K. Aagaart, R. B. Lammers, M. Steele, R. Moritz, M. Meredith, and C. M. Lee (2006), The large-scale freshwater cycle of the Arctic, *J. Geophys. Res.*, *111*, C11010, doi:10.1029/2005JC003424.

Sluijs, A., H. Brinkhuis, C. E. Stickley, J. Warnaar, G. L. Williams, M. Fuller (2003), Dinoflagellate cysts from the Eocene/Oligocene transition in the Southern Ocean; results from ODP Leg 189 [online], in *Proc. Ocean Drill. Program Sci. Results*, *189*, 1–42. (Available at http://wwwodp.tamu.edu/publications/189_SR/104/104.htm)

Sluijs, A., J. Pross, and H. Brinkhuis (2005), From greenhouse to icehouse; organic-walled dinoflagellate cysts as paleoenvironmental indicators in the Paleogene, *Earth Sci. Rev.*, *68*, 281–315.

St. John, K. (2008), Cenozoic ice-rafting history of the central Arctic Ocean: Terrigenous sands on the Lomonosov Ridge, *Paleoceanography*, *23*, PA1S05, doi:10.1029/2007PA001483.

St. John, K., and L. Krissek (2002), The late Miocene to Pleistocene ice-rafting history of southeast Greenland, *Boreas*, *31*, 28–35.

Stein, R., B. Boucsein, and H. Meyer (2006), Anoxia and high primary production in the Paleogene central Arctic Ocean: First detailed records from Lomonosov Ridge, *Geophys. Res. Lett.*, *33*, L18606, doi:10.1029/2006GL026776.

Stickley, C., N. Koç, H.-J. Brumsack, R. Jordan, and I. Suto (2008), A siliceous microfossil view of Eocene Arctic paleoenvironment: A window of biosilica production and preservation, *Paleoceanography*, doi:10.1029/2007PA001485, in press.

Thomson, D. J. (1982), Spectrum estimation and harmonic analysis, *Proc. IEEE*, *70*, 1055–1096.

Totland, M., I. Jarvis, and K. E. Jarvis (1992), An assessment of dissolution techniques for the analysis of geological samples by plasma spectrometry, *Chem. Geol.*, *95*, 35–62.

Vautard, R., and M. Ghil (1989), Singular spectrum analysis in nonlinear dynamics, with applications to paleoclimatic time series, *Phys. D*, *35*, 395–424.

Vautard, R., P. Yiou, and M. Ghil (1992), Singular-spectrun analysis: A toolkit for short, noisy chaotic signals, *Phys. D*, *58*, 95–126.

Vinje, T. (2001), Fram Strait ice fluxes and atmospheric circulation: 1950–2000, *J. Clim.*, *14*, 3508–3517.

Waddell, L. A., and T. C. Moore (2008), Salinity of the Eocene Arctic Ocean from oxygen isotope analysis of fish bone carbonate, *Paleoceanography*, doi:10.1029/2007PA001451, in press.

Walsh, J. E., X. Zhou, A. Portis, and M. C. Serreze (1994), Atmospheric contribution to hydrologic variations in the Arctic, *Atmos. Ocean*, *32*, 733–755.

Whitehead, D. R. (1983), Wind pollination: Some ecological and evolutionary perspectives, in *Pollination Biology*, edited by L. Real, pp. 97–108, Academic, Orlando, Fla.

Wood, G. D., A. M. Gabriel, and J. C. Lawson (1996), Palynological techniques—Processing and microscopy, in *Palynology: Principles and Applications*, edited by J. Jansonius and D. C. McGregor, vol. 1, chap. 3, pp. 29–50, Am. Assoc. of Stratigr. Palynol. Found., College Station, Tex.

Zachos, J., M. Pagani, L. Sloan, E. Thomas, and K. Billups (2001), Trends, rhythms, and aberrations in global climate 65 Ma to present, *Science*, *292*, 686–693.

H. Brinkhuis, F. Sangiorgi, and E. E. van Soelen, Palaeoecology, Laboratory of Palaeobotany and Palynology, Institute of Environmental Biology, Utrecht University, Budapestlaan 4, 3584 CD Utrecht, Netherlands. (f.sangiorgi@uu.nl)

N. Koç and C. E. Stickley, Norwegian Polar Institute, Polar Environmental Centre, N-9296 Tromsø, Norway.

H. Pälike and D. J. A. Spofforth, School of Ocean and Earth Science, University of Southampton, Waterfront Campus, SO17 3ZH Southampton, UK.

S. Schouten and J. S. Sinninghe Damsté, Royal Netherlands Institute for Sea Research, Department of Marine Biogeochemistry and Toxicology, P.O. Box 59, NL-1790 AB Den Burg, Texel, Netherlands.

K. St. John, Department of Geology and Environmental Science, James Madison University, MSC 6903, 7125 Memorial Hall, 395 South High Street, Harrisonburg, VA 22807, USA.